Chaos in high-dimensional neural and gene networks

Thomas Mestl [a], Chris Lemay [b], Leon Glass [b],*

[a] *Department of Mathematical Sciences, Agricultural University of Norway, PO Box 5035, N-1432 Ås, Norway*
[b] *Department of Physiology, McGill University, 3655 Drummond Street, Montréal, Qué., Canada H3G 1Y6*

Abstract

Neural and gene networks are often modeled by differential equations. If the continuous threshold functions in the differential equations are replaced by step functions, the equations become piecewise linear (PL equations). The flow through the state space is represented schematically by paths and directed graphs on an n-dimensional hypercube. Closed pathways, called *cycles*, may reflect periodic orbits with associated fixed points in a chosen Poincaré section. A return map in the Poincaré section can be constructed by the composition of fractional linear maps. The stable and unstable manifolds of the fixed points can be determined analytically. These methods allow us to analyze the dynamics in higher-dimensional networks as exemplified by a four-dimensional network that displays chaotic behavior. The three-dimensional Poincaré map is projected to a two-dimensional plane. This much simpler piecewise linear two-dimensional map conserves the important qualitative features of the flow.

1. Introduction

Complex networks are often characterized by their tremendous sizes and the nonlinear relationship between their components. A common characteristic is the occurrence of 'switch like' phenomena, i.e. intrinsic quantities may change rapidly when a threshold is crossed. For example, genes can be activated by circulatory metabolites and neurons become excited when a certain membrane potential is exceeded. For reviews stressing the importance of several types of networks see [1–3].

In order to handle networks of at least small or moderate sizes, simplified descriptions of them as switching networks or Markov processes have been developed [2,4–8]. But dynamical properties like steady states, periodicity or chaos do not always persist when passing between the different classes of models [9–13]. For instance, an attractor in synchronous switching networks may often require the simultaneous crossing of several thresholds. Such a behavior is not robust since, in general, in a continuous system only one threshold will be crossed at a time.

---

* Corresponding author.

Even though asynchronous switching avoids the simultaneous crossing of several thresholds, the problem of which pathway will be followed remains.

Previous work has explored the connections between the logical structure of model networks and their qualitative dynamics. Particular attention was focused on a class of piecewise linear (PL) equations. This class of equations is often used to describe biological systems, like gene regulatory- or neural-Hopfield networks [14–18], as well as electrical circuits [19]. A directed graph on an n-dimensional hypercube is constructed based on the logical structure of the network. The vertices on the directed graph correspond to orthants in state space and the edges correspond to transitions between orthants [11,20]. Previous work analyzed steady states [1,8,13,20,21] and limit cycles [11,12,20,22–25].

Theoretical models of gene and neural networks can also display chaotic behavior [21,26–32]. However, there is still scant theoretical insight into the origin of chaotic dynamics in these systems [26,27]. Ideally, one would wish to obtain a theoretical result that would enable us to assert whether chaotic dynamics is possible based on the logical structure of a given network. This paper attempts a more modest task. In the following we analyze chaotic dynamics in a particular four-dimensional PL equation that was discovered during searches of PL equations having random connectivities and parameters. Numerical results [30,31] and Glass (unpublished) indicate that chaotic dynamics is comparatively rare in low dimensions – of the order one network per 1000 randomly generated networks in four dimensions.

Because of the simple nature of the PL equations, significant analysis is possible. In Section 2 we present the general class of equations under consideration. We review earlier work that gives analytic formulae for the integration of these equations. Section 3 presents the specific four-dimensional PL equation displaying chaotic dynamics. We present numerical simulations and emphasize the inadequacy of Boolean or Markovian approaches to capture the dynamics in the continuous four-dimensional state space. Section 4 presents general theoretical results for the class of PL equations. We show how one can analytically compute the Poincaré section, the fixed points in the Poincaré section, and the stable and unstable manifolds of fixed points. Section 5 applies the analytical methods to the specific example presented in Section 3. We compute the Poincaré map, show how to project it to two dimensions, and analyze the stable and unstable manifolds in this two-dimensional projection. We analytically compute a transverse homoclinic intersection. Moreover, we show that the attractor is dominated by a strong attraction to the unstable manifold of a fixed point. The general features of the two-dimensional map are captured in a simplified example which is presented in Section 6. We discuss the implications of the work in Section 7.

2. Mathematical background

In this section we summarize the flows in the PL equations based on [11,12]. Let x_i be a continuous variable denoting the gene product concentration of gene i or the membrane potential of neuron i. Let X_i be a Boolean variable called the *activity*, defined as follows: if $x_i > 0$ the gene or neuron activity is $X_i = 1$, whereas if $x_i < 0$ then $X_i = 0$, i.e. at $x_i = 0$ the activity has a threshold.

Throughout the article we consider the general class of systems given by coupled first-order autonomous differential equations

$$\frac{dx_i}{dt} = \alpha_i(X) - \gamma(X)x_i, \quad i = 1, \ldots, n, \tag{2.1}$$

where $\alpha_i(X)$ and $\gamma(X)$ are piecewise constant functions whose values may change as the variables x_j crosses their thresholds. We use boldface to represent arrays. The relative destruction rates $\gamma(X)$ are always positive and are

taken to be equal for all variables in state X, hence $\gamma(X)$ is without index i. Since $\gamma(X)$ is the same for all variables in state X, the trajectories are piecewise straight lines in the state space.

The thresholds divide the state space into rectangular open orthants, called *boxes*. The number of boxes in an n-dimensional system is 2^n. The unique labeling of a box is given by the corresponding activity $X = X_1 X_2 \cdots X_n$. For instance, the region $\{x_1 > 0, x_2 < 0, \ldots, X_{n-1} < 0, x_n > 0\}$ gives the box $(10\ldots01)$, whereas $\{x_1 > 0, x_2 < 0, \ldots, x_n < 0$, gives $(10\ldots0)$.

Inside a box the system evolves along a straight line which is directed towards a *focal point*, $f(X) = [f_1 \ldots, f_n]$ [11]. The focal point coincides with the steady-state solution with the given parameter values valid in the box, i.e. $f_i(X) = \alpha_i(X)/\gamma(X)$. No matter where the system starts in that box all trajectories would meet at this point if they did not enter an adjacent box. Consequently, the location of the focal point of a box with respect to adjacent boxes determines which of them can in principle be entered.

The partition of the state space into boxes and the fact that inside such a box the system equation (Eq. (2.1)) is a first-order linear differential equation with *nonvarying* parameters, allows a piecewise analytical integration of $dx_i/dt = \alpha_i(X) - \gamma(X)x_i$. The solution expressed in terms of $f_i = f_i(X)$ and $\gamma = \gamma(X)$ in box X is

$$x_i(t) = f_i + (x_i(0) - f_i)e^{-\gamma t}, \tag{2.2}$$

where $x_i(0)$ is the starting value ($t = 0$) inside a certain box.

With this partition of the state space, trajectories are always straight lines inside a box. However, they may show corners at the interface between two adjacent boxes. This interface is a part of a threshold or hyperplane, and will simply be called a *wall* $\mathcal{W} \in \mathbb{R}^{n-1}$. For instance, the wall between box $10\ldots01$ and box $10\ldots0$ is $\mathcal{W} = \{x_1 > 0, x_2 < 0, \ldots, x_{n-1} < 0, x_n = 0\}$.

Now, suppose the trajectory leaves a box through threshold wall $x_j = 0$. Solving the corresponding equation with respect to time (the transit time is t^* through that box) and substituting t^* into the remaining equations eliminates time from all equations. The intersection point (denoted by y) with the 'exit' wall can either be given in component form

$$y_i = \frac{x_i(0) - (f_i/f_j)x_j(0)}{1 + x_j(0)/(-f_j)}, \tag{2.3}$$

or in vector notation [11]

$$y = M(x) = \frac{Cx(0)}{1 + c^t x(0)}, \tag{2.4}$$

where matrix $C \in \mathbb{R}^{n \times n}$. The vector $c^t \in \mathbb{R}^n$ has zero elements except $c_j = -1/f_j$, and is transposed. If no focal point is located exactly in the walls of its box then $c^t x > 0$ always. Eq. (2.4) is called a fractional linear map.

The domain of definition of $M(x)$ is restricted to the region in wall $\mathcal{W}$ given by the backwards mapping of a particular exit wall on $\mathcal{W}$. This is because starting at a different place in $\mathcal{W}$ the system may leave the box through a different exit wall. If the box is left through a single exit wall only, then $M(x)$ is valid every where in $\mathcal{W}$.

The flows from box to box are computed by the composition of fractional linear maps. Since the composition of two fractional linear maps is again a fractional linear map, significant analysis of the flows is sometimes possible since the dynamics can be reduced to a matrix multiplication [11,12]. Consequently, the trajectories have a simple analytical representation.

A convenient way of visualizing the state space is by representing it as a *hypercube*, where each vertex denotes a box and each edge represents the walls between adjacent boxes, Fig. 1. Starting in a box the corresponding parameter values, α and γ, determine whether or not an adjacent box can be entered. Thus we assign an arrow to each edge indicating whether at least some trajectories in a box can reach the corresponding adjacent box. The resulting directed graph is called a state transition diagram. The possible transitions between boxes may either be
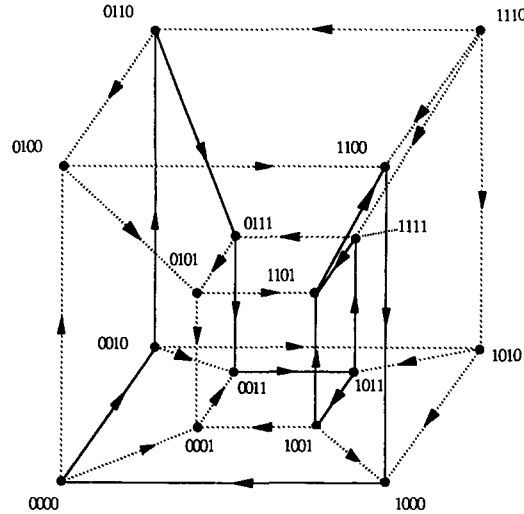
Fig. 1. The state transition diagram for the PL equation in Eq. (3.1). The vertices correspond to boxes and directed edges represent allowed transitions between adjacent boxes. There are 29 cycles (four 4-vertex, six 6-vertex, ten 8-vertex and nine 10-vertex cycles.

visualized as an arrow on an edge of the hypercube, or may be given as a truth table specifying a possible next state, cf. Table 1. If the sign of $\alpha_i(X)$ is not a function of X_i, then each edge in the state transition diagram is oriented in one and only one direction [11].

3. Numerical studies of a four-dimensional system

In this paper we consider the following four-dimensional ordinary differential equation,

$$
\begin{aligned}
dx_1/dt &= 2(X_2\bar{X}_3 + \bar{X}_2 X_3) - 1.2546 - x_1, \\
dx_2/dt &= 2(\bar{X}_1\bar{X}_4 + X_1 X_4) - 1.3762 - X_2, \\
dx_3/dt &= 2\bar{X}_1\bar{X}_2 - 0.8024 - x_3, \\
dx_4/dt &= 2(\bar{X}_1\bar{X}_3 + X_3) - 1.2682 - x_4,
\end{aligned}
\tag{3.1}
$$

where $\bar{X}_i = 1 - X_i$. Note that $\gamma(X)$ is equal to 1 for all x_i resulting in straight lines in the state space. The network and parameter values were found when numerically searching for irregular behavior in randomly generated systems, and have no direct biological interpretation.

The Boolean equation, Eq. (3.2), represents the logical structure of our model example Eq. (3.1) as

$$
\begin{aligned}
X_1^{(k+1)} &= X_2^{(k)}\bar{X}_3^{(k)} + \bar{X}_2^{(k)} X_3^{(k)}, \\
X_2^{(k+1)} &= \bar{X}_1^{(k)}\bar{X}_4^{(k)} + X_1^{(k)} X_4^{(k)}, \\
X_3^{(k+1)} &= \bar{X}_1^{(k)}\bar{X}_2^{(k)}, \\
X_4^{(k+1)} &= \bar{X}_1^{(k)}\bar{X}_3^{(k)} + X_3^{(k)},
\end{aligned}
\tag{3.2}
$$

where the superscript $(k+1)$ gives the next activity stage. By iteration we find that the synchronous switching system, Eq. (3.2), always reaches the cycle $1011 \rightarrow 1101 \rightarrow 1100 \rightarrow 1000 \rightarrow 0000 \rightarrow 0111 \rightarrow 0001 \rightarrow 0011 \rightarrow 1011$. The truth table for this switching network is given in Table 1. Table 1 also contains the transition probabilities between boxes when restarting randomly each time in a box, i.e. assuming a Markov process as in Rigney [7], see Appendix A.

Table 1

| From | To | | Transition | Stationary |
	Synchr.	Asynchr.	probability	distribution
0000	0111	0001	0.2866	0.1065
		0010	0.4691	
		0100	0.2443	
0001	0011	0011	1.0000	0.0820
0010	1111	0011	0.3483	0.0500
		0110	0.2969	
		1010	0.3548	
0011	1011	1011	1.0000	0.1266
0100	1101	0101	0.4954	0.0338
		1100	0.5046	
0101	1001	0001	0.6487	0.0326
		1101	0.3513	
0110	0101	0100	0.5230	0.0148
		0111	0.4770	
0111	0001	0011	0.6317	0.0431
		0101	0.3683	
1000	0000	0000	1.0000	0.1065
1001	0100	0001	0.3987	0.0760
		1000	0.4030	
		1101	0.1982	
1010	1001	1000	0.5230	0.0177
		1011	0.4770	
1011	1101	1001	0.5626	0.1351
		1111	0.4374	
1100	1000	1000	1.0000	0.0666
1101	1100	1100	1.0000	0.0496
1111	1010	0111	0.6099	0.0591
		1101	0.3901	
1110	0001	0110	0.3012	0.0000
		1010	0.3304	
		1100	0.1927	
		1111	0.1757	

Note. Columns 2 and 3 are the successor states of the vertices of column 1 in case of synchronous and asynchronous switching, respectively. Column 4 gives the transition probabilities for a Markov model based on the location of the focal points, whereas column 5 contains the stationary densities of the Markov model for each state in column 1.

A more convenient way of displaying the dynamics of system Eq. (3.1) is given by the state transition diagram, see Fig. 1. The focal point f_1 of variable x_1 is either $f_1^- = -1.2546$ or $f_1^+ = 2 - 1.2546$, depending on the state X. A similar definition for the focal points f_i holds for the other x_i. Thus, in box (0000) the focal point is $f = [f_1^-, f_2^+, f_3^+, f_4^+]$ indicating a forthcoming crossing of the x_2, x_3 and/or x_4 threshold.

From the figure or the truth table it can immediately be seen that box (1110) can never be entered, i.e. all arrows point outward, hence no closed trajectory can pass through the corresponding part of the state space. If there exist closed trajectories in the differential equations they must be contained in a certain properly connected box sequence. A *cycle* (or circuit in graph theory) is a path on the hypercube leading back to the starting vertex but without entering a vertex twice. A closed trajectory must be contained in a cycle or the union of connected cycles.

By successively applying Eq. (2.4) a trajectory can be followed, see Fig. 2(a). Simulations show that the system will, after a transient period, usually traverse two cycles, called $\mathcal{A}$ and $\mathcal{B}$, which are emphasized in bold in Fig. 1.

$\mathcal{A}$: $1011 - \mathbf{1111} - 1101 - 1100 - 1000 - 0000 - 0010 - 0110 - 0111 - 0011$
$\mathcal{B}$: $1011 - \mathbf{1001} - 1101 - 1100 - 1000 - 0000 - 0010 - 0110 - 0111 - 0011$

These two cycles differ only in one vertex (bold number) and no more than one threshold is crossed at a time (in comparison to the result from the synchronous switching approach [2,4,10,11]). In order to examine the dynamics more closely, the threshold wall between box (0011) and (1011) was chosen as a Poincaré section, i.e. the part of the phase space defined by the wall $\mathcal{W} = \{x_1 = 0, \ x_2 < 0, \ x_3 > 0, \ x_4 > 0\}$. This three-dimensional section is divided by a 'separating boundary' $\mathfrak{b}$ into two domains $\mathcal{A}$ and $\mathcal{B}$, so that when starting in domain $\mathcal{A}$ the system will traverse cycle $\mathcal{A}$, whereas starting in domain $\mathcal{B}$, cycle $\mathcal{B}$ is traversed.

A *strange attractor* of Eq. (3.1) emerges when plotting successive iterations on the Poincaré section, Fig. 2(b), or when plotting $x_2^{(k+1)}$ as a function of $x_2^{(k)}$ on this wall, Fig. 2(c). Simulations show that the system alternates
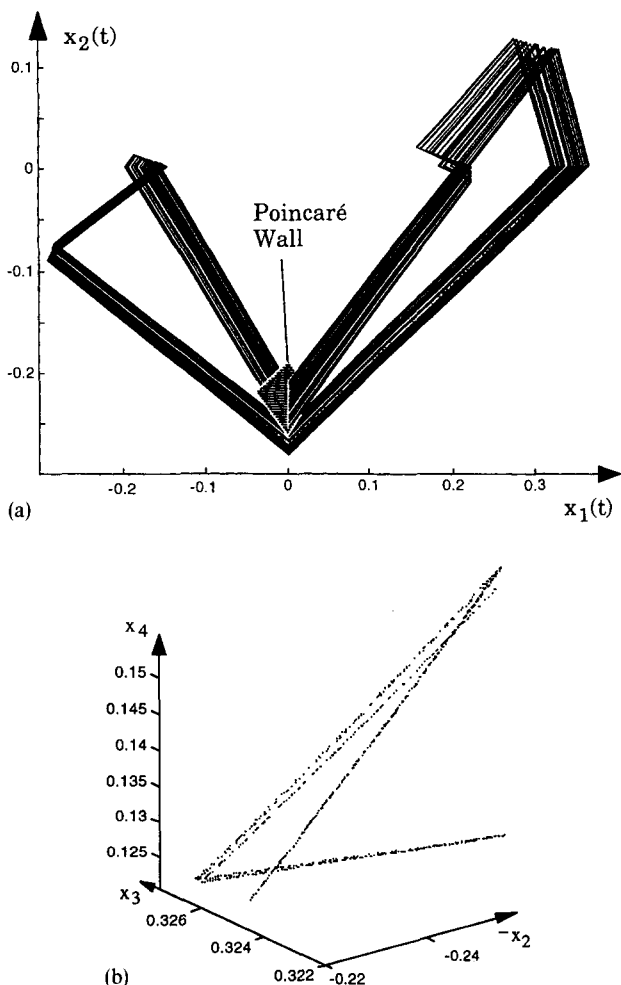

Fig. 2. (a) The attractor of the system projected on the x_1–x_2-plane. For clarity only 40 transitions through cycle $\mathcal{A}$ and $\mathcal{B}$ are plotted. (b) The intersection points of the chaotic attractor of Eq. (3.1) with the wall between boxes (0011) and (1011) defined by $\mathcal{W} = \{x_1 = 0, \ x_2 < 0, \ x_3 > 0, \ x_4 > 0\}$. (c) The return map of $x_2^{(k+1)}$ as a function of $x_2^{(k)}$ resembles a 'tent map'. All computations are performed in Matlab.
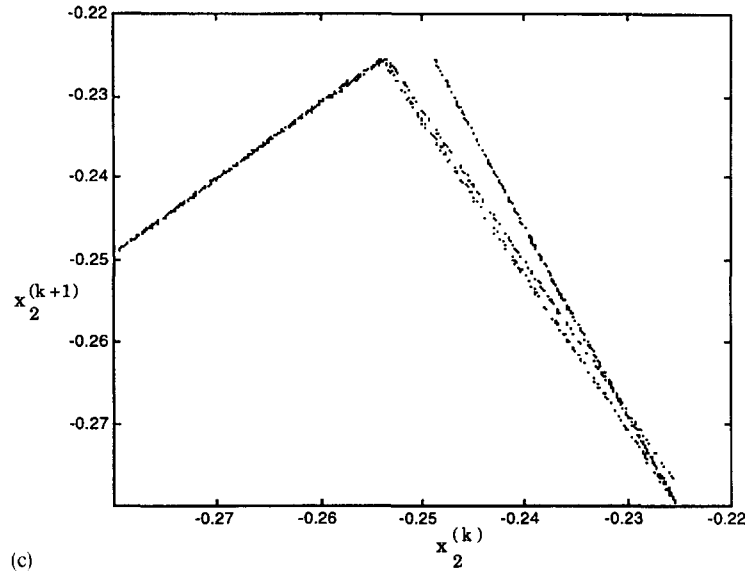
(c)

Fig. 2. Continued

irregularly between cycle $\mathcal{A}$ and $\mathcal{B}$. Two $\mathcal{B}$'s never followed each other in the sequence, whereas cycle $\mathcal{A}$ was traversed several times in succession.

The Lyapunov exponents are related to the average rates of convergence and/or divergence of nearby trajectories. It is thus a measure of the predictability of a system. The number of Lyapunov exponents equals the dimension of the system. These exponents are given by

$$h = h(x^{(0)}, u^{(0)}) = \lim_{N \to \infty} \frac{1}{N} \ln \left(|J^{(N)} \cdot u^{(0)}| \right),$$

where

$$J^{(N)} = \frac{\partial M}{\partial x} \bigg|_{x^{(N-1)}} \cdots \frac{\partial M}{\partial x} \bigg|_{x^{(0)}}$$

(for $\frac{\partial M}{\partial x}$ see Section 4) is the product of the Jacobians and $u^{(0)}$ is an initial perturbation. For large N the Lyapunov exponents are approximated by

$$h(x^{(0)}, u^{(0)}) \cong \frac{1}{2N} \ln \left[\left(u^{(0)} \right)^t H^{(N)} u^{(0)} \right],$$

where $H^{(N)} = \left(J^{(N)} \right)^t J^{(N)}$ is a real nonnegative hermitian matrix [33]. The eigenvalues e_i of $H^{(N)}$ approximates the Lyapunov exponents, i.e. $h_i = (1/2N) \ln e_i$. An operational definition for chaos is that at least one Lyapunov number is positive in a bounded system. In our example the dynamics are bounded and the largest Lyapunov exponent is approximately 0.45. Thus, the system is chaotic.

The rest of this paper deals with the theoretical analysis of this example. In Section 4 we present general results concerning the fixed points of the fractional linear map. Then in Section 5 we apply these results to our specific example given by Eq. (3.1).

4. Fixed points and their stable and unstable manifolds

In this section we present properties of fractional linear maps derived from differential equations given by Eq. (2.1). Eq. (2.4) gave the mapping $M(x)$ from a starting point x in a wall, through the box in the direction of the focal point, to the intersection point y with another threshold wall. The mapping Eq. (2.4), $M(x) : x \rightarrow y$ has a unique inverse $M^{-1}(y)$,

$$x = M^{-1}(y) = \frac{C^{-1}y}{1 - c^t C^{-1}y},\tag{4.1}$$

where matrix $C \in \mathbb{R}^{n \times n}$ and vector $c \in \mathbb{R}^n$ is entirely determined by the focal point f of that box.

4.1. Closed trajectory = fixed point of the return map

If there exist closed trajectories then they have to be contained in a properly connected box sequence, i.e. a cycle or a union of connected cycles. The flow associated with a cycle $\mathcal{A}$ in state space can be traced by the successive application of the corresponding maps. Then choosing the threshold wall $\mathcal{W} = \mathcal{W}(x_j = 0)$ as the Poincaré cross section we obtain a return map $M_{\mathcal{A}}(x)$ for the cycle $\mathcal{A}$:

$$M_{\mathcal{A}}(x) = \frac{Ax}{1 + a^t x},\tag{4.2}$$

where matrix $A \in \mathbb{R}^{(n-1) \times (n-1)}$ and vector $a \in \mathbb{R}^{(n-1)}$ are specific for cycle $\mathcal{A}$. They are of lower dimension since the row and column corresponding to x_j can be deleted. In [12] an efficient way of computing A and a is presented. As before the domain of definition of map $M_{\mathcal{A}}(x)$ is not necessarily the whole Poincaré cross section, but only that part of $\mathcal{W}$ in which the trajectories do not leave cycle $\mathcal{A}$.

If a closed trajectory is associated with cycle $\mathcal{A}$ then the return map $M_{\mathcal{A}}(x)$ has a fixed point where the trajectory intersects the Poincaré section. A fixed point F_i of the return map $M_{\mathcal{A}}(x)$ must lie on an eigenvector v_i with eigenvalue λ_i of A, i.e. $F_i = \kappa_i v_i$ with $\kappa_i > 0$, and must in addition be contained in the Poincaré section. Throughout the article only real and distinct eigenvalues are assumed. From Eq. (4.2) combined with $F_i = \kappa_i v_i$, an expression for κ_i can be derived,

$$\kappa_i = \frac{\lambda_i - 1}{a^t |v_i| = 1}.\tag{4.3}$$

Observe from Eq. (4.2) that $x = 0$ will always be a fixed point of $M_{\mathcal{A}}(x)$. The problem of finding periodic orbits in large nets is therefore reduced to identifying cycles on the hypercube and solving the corresponding eigenvalue problems.

4.2. Necessary requirements for existence of a fixed point

Several properties of a fixed point can be deduced from its eigenvalue. However, a fixed point of a return map $M_{\mathcal{A}}(x)$ does not necessarily represent a closed trajectory since it may lie outside the Poincaré section or its existence may violate the requirement of boundedness of solutions. Since the system evolves towards a focal point it must enter the bounded domain given by $|x| \leq \max |f|$, where the maximum is taken over all f.

Theorem 1. No closed trajectory can pass through a fixed point $F_i = \kappa_i v_i$ on an eigenvector v_i with an eigenvalue less than one.

Proof. The simplest way to show this is by using the argument of boundedness. Let F_i be a fixed point on v_i (but not the origin). Assume $\lambda_i < 1$. From Eq. (4.3) it follows that $a^t F_i = \lambda_i - 1$, which is negative, Thus, for $x = F_i/(1 - \lambda_i)$, $M(x)$ in Eq. (4.3) is singular, which is impossible. Consequently, we cannot have a fixed point.

In case $\lambda_i = 1$ the origin is attracting since $a^t v_i > 0$.

However, $\lambda_i > 1$ and $v_i \in$ Poincaré section, is only a necessary, but not sufficient requirement for the existence of a closed trajectory. □

4.3. The Jacobain and stability of fixed points

The Jacobain at any point x is given by

$$J(x) = \frac{1}{1 + a^t x} \left(A - \frac{Ax}{1 + a^t x} a^t \right).$$

At a fixed point F_i on the eigenvector v_i with eigenvalve λ_i the Jacobian $J(F_i)$ becomes

$$J(F_i) = \frac{1}{\lambda_i} \left(A - F_i a^t \right). \tag{4.4}$$

The eigenvectors and eigenvalues of the Jacobian $J(F_i)$ are

Eigenvector : F_i,   Eigenvalue : $1/\lambda_i$, $\qquad\qquad\qquad\qquad\qquad\qquad$ (4.5a)

Eigenvector : $(F_j - F_i)$,   Eigenvalue : λ_j/λ_i, $\qquad\qquad\qquad\qquad$ (4.5b)

where $(F_j - F_i)$ is the direction from F_i to the other fixed points F_j, and λ_j is the eigenvalue of F_j (Eq. (4.3)).

Theorem 2. A necessary and sufficient requirement for stability of F_i is that $\lambda_i > \max |\lambda_j|$, for $j \neq i$. If $0 < \lambda_i < 1$ the origin becomes attracting along v_i.

This follows from Eq. (4.5) and the fact that a fixed point of a map is stable only if the magnitude of the largest eigenvalue of the Jacobian evaluated at the fixed point is less than one.

4.4. Manifolds and their representation

The stable and unstable manifolds at a fixed point F_i of cycle $\mathcal{A}$ are denoted by $W^s_\mathcal{A}(F_i)$ and $W^u_\mathcal{A}(F_i)$, respectively. The manifolds of fixed points of fractional linear maps are linear spaces spanned by the eigenvectors of the corresponding Jacobian. Assuming distinct and real eigenvalues, then the manifolds are

$$\begin{aligned} W^s_\mathcal{A}(F_i) &= \text{span} \{F_i, (F_j - F_i)\}, \quad j \text{ such that } |\lambda_j|/\lambda_i < 1, \\ W^u_\mathcal{A}(F_i) &= F_i + \text{span} \{(F_k - F_i)\}, \quad k \text{ such that } |\lambda_k|/\lambda_i > 1. \end{aligned} \tag{4.6}$$

Note that in case $W^u_\mathcal{A}$ is one-dimensional then it is given by a line from F_i to F_k, embedded in the space spanned by $(F_k - F_i)$. In case $W^u_\mathcal{A}$ is two-dimensional then it is given by a plane through F_i spanned by $(F_k - F_i)$.

Depending on the values of the eigenvalues, a fixed point can be hyperbolic or nonhyperbolic, stable and unstable, and if eigenvalues have negative sign, reflection occurs in the corresponding manifold.

4.5. A further reduction of the Poincaré map

Once an eigenvector of $M_\mathcal{A}(x)$ is found, the corresponding fixed point F_i can immediately be determined with Eq. (4.3). This suggests that the $(n - 1)$-dimensional return map of the Poincaré section can be reduced even further
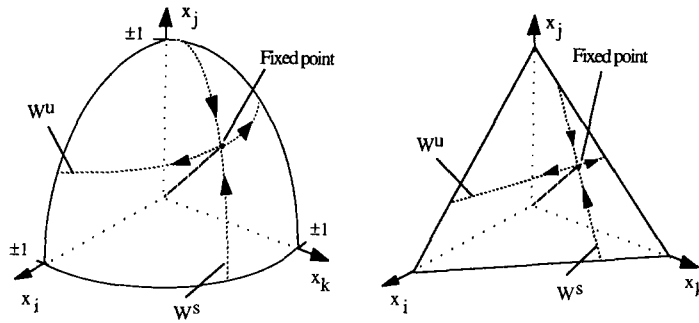
Fig. 3. Linear automorphism on a sphere and on a proper transversal plane in a three-dimensional Poincaré section where manifolds are represented either by chords or line segments.

to a $(n-2)$-dimensional map. In order to perform this reduction we need first two important properties of fractional linear maps.

Consider two points, x_1 and x_2, on an arbitrary vector v, i.e. $x_1 = \kappa_1 v$ and $x_2 = \kappa_2 v$, $\kappa_i > 0$ for $i = 1, 2$ (a ray is defined as the family of points, x_i, where $x_i = \kappa_i v$ for all $\kappa_i > 0$). Applying the fractional linear map $M_{\mathcal{A}}$ from Eq. (2.4) these points are mapped to $x_1^{(1)}$ and $x_2^{(1)}$, respectively, $x_i^{(1)} = M_{\mathcal{A}}(x_i) = \kappa_i Av/(1 + \kappa_i a^t v)$. Note that $x_1^{(1)}$ and $x_2^{(1)}$ lie on the same iterated vector, i.e. Av. This reveals the important property that all points on a ray map to the same ray under successive mapping.

Theorem 3. The distance between two points x and $y = \kappa x, \kappa > 1$, on any iterated ray x will go to zero as the number of iterations goes to infinity.

Proof. From Eq. (2.3) or Eq. (2.4) it can be deduced that if no focal point is lying on a threshold then $c^t x > 0$ always. Assume the system traverses through an arbitrary sequence of boxes $S = \{1, 2, \ldots, k\}$ then the mapping is given by the composed fractional linear map $M_S(x) = S_k x/(1 + s^t x)$, where $S_k = C_k \ldots C_2 C_1$ is the product of the individual mapping matrices, and $s^t x = (c_1^t x + c_2^t C_1 x + \cdots + c_k^t S_{k-1} x)$. Note that $s^t x$ goes to + infinity when $k \to \infty$. Therefore, in the limit $k \to \infty$

$$\lim_{k \to \infty} \left| \frac{x^{(k)}}{y^{(k)}} \right| = \lim_{s^t x \to \infty} \frac{1 + \kappa s^t x}{\kappa(1 + s^t x)} = 1. \tag{4.7}$$

That is, all points on a ray either approach the origin, or approach a nonzero asymptotic trajectory.   □

Since all trajectories starting on a vector span a two-dimensional piecewise plane surface in the state space, the order of the iterated points on the vector will persist because trajectories cannot cross each other. In [12] this and the fact that this surface cannot intersect itself was used to deduce the chaos cannot occur in three-dimensional systems given by Eq. (2.1). Aperiodic dynamics may however be possible in higher dimensions.

Now consider the intersection of iterates of a ray with a hypersurface S of dimension $(n-2)$ that is transverse to the rays in a Poincaré section, Fig. 3. This projection preserves essential features of the dynamics. For instance, one can assume that S is a unit sphere, to generate a linear automorphism on a sphere [34], i.e. $M^r(x) = Ax/|Ax|$, where $M^r(x)$ is a reduced map.

A ray is represented in this $(n-2)$-dimensional surface S as a point. That is, iterations give a sequence of points on this surface S which may approach the fixed point. The intersection of $W_{\mathcal{A}}^S(F_i)$, from Eq. (4.6), with this surface S gives the representation of the stable manifold of a fixed point in S. The representation of the unstable manifold $W_{\mathcal{A}}^u$ in S, is defined by the intersection of span $\{F_i W_{\mathcal{A}}^u(F_i)\}$, see Fig. 3.

To analyze our four-dimensional example, we will take the projection on a plane rather than on a unit sphere. This is more convenient since this results in pieces of straight lines representing manifolds instead of chord pieces, see Fig. 3.

5. Theoretical analysis of the model system (Eq. (3.1))

The numerical simulations of Section 3 indicated the occurrence of aperiodic chaotic dynamics since there was a positive Lyapunov number. Based on the theory developed in the preceding section we will explore the dynamical properties of the model.

5.1. Stationary point

Before dealing with the chaotic dynamics we note that system (Eq. (3.1)) contains one stable fixed point at $(0; -0.1786; 0; 0.2855)$ which is attracting and located on a threshold intersection. Trajectories spiral towards this point by traversing the cycle 0011–1011–1001–0001. This fixed point can be identified either by the method presented in [13,21], or by composing the corresponding linear fractional map and determining its fixed points.

5.2. Periodic solutions

In order to find possible periodic solutions the wall between box (0011) and (1011), $\mathcal{W} = \{x_1 = 0, x_2 < 0, x_3 > 0, x_4 > 0\}$, was chosen as Poincaré section. This wall is common to cycles $\mathcal{A}$ and $\mathcal{B}$ as given in Section 3. If $x_2 > -0.7774 x_3$ the system follows cycle $\mathcal{A}$, otherwise it follows cycle $\mathcal{B}$. Therefore, the plane $x_2 + 0.7774 x_3 = 0$ separates the domain of cycle $\mathcal{A}$ and the domain of cycle $\mathcal{B}$. Assume the system starts exactly at this separating boundary $\mathfrak{b}$ in $\mathcal{W}$. Then it proceeds through box (1011) towards box (1111) as well as to box (1001), and hence must leave box (1011) in the set $\{x_1 > 0, x_2 = 0, x_3 = 0, x_4 > 0\}$. Since this set is common for both boxes and hence for both cycles, and the cycles join again in the following box (1101), the mapping is continuous at the separating boundary $\mathfrak{b}$. This is a general property of two cycles differing only in one vertex.

The return map

$$M_\mathcal{A}(x) = \frac{Ax}{1 + a^\mathfrak{t} \cdot x} \quad \text{and} \quad M_\mathcal{B}(x) = \frac{Bx}{1 + b^\mathfrak{t} \cdot x}$$

of cycle $\mathcal{A}$ and $\mathcal{B}$ are constructed as indicated in Section 4, and are given in Table 2 together with their fixed points and eigenvalues.

By applying Theorem 1 we know that no closed trajectory can pass through points on eigenvectors with $\lambda_i < 1$. The attracting fixed point $F_{\mathcal{A}1}$ lies inside $\mathcal{B}$-domain, and $F_{\mathcal{B}1}$ lies inside $\mathcal{A}$-domain. The fixed points $F_{\mathcal{A}2}$ and $F_{\mathcal{B}2}$ lie outside the Poincaré cross section. Consequently, there are only period one orbits through the fixed points $F_{\mathcal{A}3}$ and $F_{\mathcal{B}3}$.

Since $|\lambda_{\mathcal{A}1}| > \lambda_{\mathcal{A}3} > |\lambda_{\mathcal{A}2}|$ and $\lambda_{\mathcal{A}1}, \lambda_{\mathcal{A}2}$ are both negative, $F_{\mathcal{A}3}$ is an unstable, hyperbolic fixed point with reflection in the unstable and stable manifolds, $W_\mathcal{A}^\mathrm{u}$ and $W_\mathcal{A}^\mathrm{s}$. The ustable maniflod $W_\mathcal{A}^\mathrm{u}$ is one-dimensional and is defined by the line through $F_{\mathcal{A}1}$ and $F_{\mathcal{A}3}$, whereas $W_\mathcal{A}^\mathrm{s}$ is a two-dimensional subspace spanned by $F_{\mathcal{A}3}$ and $F_{\mathcal{A}2}$, see Eq. (4.6).

Since $\lambda_{\mathcal{B}1} > \lambda_{\mathcal{B}3} > \lambda_{\mathcal{B}2}$, $F_{\mathcal{B}3}$ is an unstable, hyperbolic fixed point without reflection in its manifolds.

5.3. Reduction to a plane

As indicated in Section 4.5 the fractional linear map in the Poincaré section can be reduced by projecting the return map to the plane that contains the fixed point $F_{\mathcal{A}3}$ and having $F_{\mathcal{A}3}$ as normal vector. The reduction on this plane,

Table 2
The parameter values of the mapping matrices corresponding to cycles $\mathcal{A}$ and $\mathcal{B}$ with their associated fixed points and eigenvalues of A and B

Cycle $\mathcal{A}$	Cycle $\mathcal{B}$
$A = \begin{bmatrix} -10.61485 & -9.80490 & -3.45291 \\ 2.10586 & 4.74710 & 2.99121 \\ 6.39551 & 5.77126 & 1.93463 \end{bmatrix}$	$B = \begin{bmatrix} 0.40189 & -1.24076 & -3.45291 \\ 4.74344 & 6.79749 & 2.99121 \\ -0.26499 & 0.59355 & 1.93463 \end{bmatrix}$
$a^t = \begin{bmatrix} 4.92075 & 11.49434 & 6.26952 \end{bmatrix}$	$b^t = \begin{bmatrix} 9.78782 & 15.27787 & 6.26952 \end{bmatrix}$

Eigenvalues of A:

$\lambda_{\mathcal{A}1}$	$\lambda_{\mathcal{A}2}$	$\lambda_{\mathcal{A}3}$
−8.2927	−0.0275	4.3871

Eigenvalues of B:

$\lambda_{\mathcal{B}1}$	$\lambda_{\mathcal{B}2}$	$\lambda_{\mathcal{B}3}$
5.6530	0.0516	3.4294

Fixed Points of $M_{A3}(x)$:

$F_{\mathcal{A}1}$	$F_{\mathcal{A}2}$	$F_{\mathcal{A}3}$
$\begin{bmatrix} 0 \\ -11.13411 \\ 0.23044 \\ 6.83240 \end{bmatrix}$	$\begin{bmatrix} 0 \\ 0.44330 \\ -0.84214 \\ 1.03219 \end{bmatrix}$	$\begin{bmatrix} 0 \\ -0.244217959 \\ 0.3269031657 \\ 0.1325688415 \end{bmatrix}$

Fixed Points of $M_B(x)$:

$F_{\mathcal{B}1}$	$F_{\mathcal{B}2}$	$F_{\mathcal{B}3}$
$\begin{bmatrix} 0 \\ -0.31331 \\ 0.28970 \\ 0.17060 \end{bmatrix}$	$\begin{bmatrix} 0 \\ 0.81229 \\ -0.72284 \\ 0.34212 \end{bmatrix}$	$\begin{bmatrix} 0 \\ -0.12891 \\ 0.35971 \\ 0.06667 \end{bmatrix}$

in the following called the 2D-plane, will remove all movement in the F_{A3} direction. The separating boundary $\mathfrak{b}$ between the $\mathcal{A}$ and $\mathcal{B}$ domains in the Poincaré section intersects the 2D-plane in a straight line.

To simplify the representation we change the basis so that the fixed-point vectors of $M_A(x)$ give the new basis vectors. With help of the transformation matrix $T = [-F_{\mathcal{A}1} \; F_{\mathcal{A}2} \; F_{\mathcal{A}3}]$ the old basis x can be expressed in terms of the new ones $y = T^{-1}x$. In the new coordinates, $W_{\mathcal{A}}^s$ and $W_{\mathcal{A}}^u$ becomes the vertical and horizontal axis, respectively. Fig. 4(a) gives a schematic picture of the dynamics occurring in this 2D-plane. Since $F_{A3} \in$ 2D-plane, $y_3 = 1$ always. The reduced iteration map $y^{(k+1)} = M_{\mathcal{A}}^r(y^{(k)})$ in the $\mathcal{A}$-domain expressed in the new coordinates is then specified by the eigenvalues of A, i.e.

$$y^{(k+1)} = \begin{bmatrix} \lambda_{\mathcal{A}1}/\lambda_{\mathcal{A}3} & 0 \\ 0 & \lambda_{\mathcal{A}2}/\lambda_{\mathcal{A}3} \end{bmatrix} y^{(k)} \cong \begin{bmatrix} -1.8898 & 0 \\ 0 & -0.0063 \end{bmatrix} y^{(k)}, \tag{5.1a}$$

where $y = [y_1, y_2]^t$.

To obtain the reduced map $M_{\mathcal{B}}^r(y)$ for cycle $\mathcal{B}$ its corresponding B matrix has first to be transformed into the new coordinates, $B^* = T^{-1}BT$, and then y_3 must be restricted to $y_3 = 1$. The reduced two-dimensional map $M_{\mathcal{B}}^r(y)$ can then be written as

$$y^{(k+1)} = \frac{\begin{bmatrix} b_{11} & b_{12} \\ b_{21} & b_{22} \end{bmatrix} y^{(k)} + \begin{bmatrix} b_{13} \\ b_{23} \end{bmatrix}}{b_{33} + [b_{31} \; b_{32}] \cdot y^{(k)}} \cong \frac{\begin{bmatrix} 4.7222 & -0.2511 \\ 2.2053 & -0.0700 \end{bmatrix} y^{(k)} + \begin{bmatrix} 0.0118 \\ 0.0020 \end{bmatrix}}{4.4814 + [103.27 - 1.9928] \cdot y^{(k)}}, \tag{5.1b}$$

where b_{ij} gives the (i, j)th element in the B^* matrix.

To give a complete representation in the 2D-plane the separating boundary $\mathfrak{b}$ has to be intersected with the 2D-plane giving the boundary line $\mathfrak{b}$: $y_1 = -9.0924 \times 10^{-4} + 0.0193y_2$. In Fig. 4(a), if the system is to the right of $\mathfrak{b}$ then $M_{\mathcal{A}}^r(y)$ has to be applied. Otherwise $M_{\mathcal{B}}^r(y)$ is used.
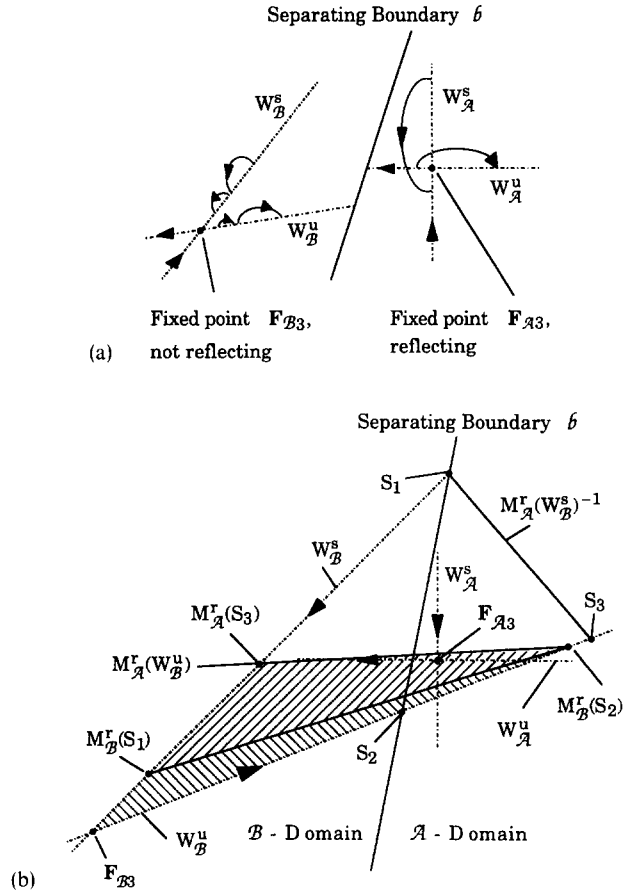
Fig. 4. (a) The dynamics around the fixed points on the 2D-plane, Eq. (5.1). (b) The triangular region in $\mathcal{A}$-domain with corners S_1, S_2 and S_3 is mapped onto the right hatched region, whereas the triangular region in $\mathcal{B}$-domain with corners S_1, S_2 and $F_{\mathcal{B}3}$ is maped onto the left hatched region. The union of the hatched regions represent a trapping region in the 2D-plane. It contains the fixed point $F_{\mathcal{A}3}$.

5.4. There exists a trapping region around $F_{\mathcal{A}}$

From the simulations of Section 3.3 it was obvious that the system is trapped 'close' to $F_{\mathcal{A}}$. To show this, consider Fig. 4(b) which schematically visualizes the manifolds with some of their mappings. First consider the $\mathcal{B}$-domain. $W_{\mathcal{B}}^s$ intersects the separating boundary b at S_1, and $W_{\mathcal{B}}^u$ intersects the separating boundary b at S_2. The triangular region defined by $F_{\mathcal{B}3}$, S_1 and S_2 maps to the left hatched region. Now consider the $\mathcal{A}$-domain. S_3 is the intersection point of $M_{\mathcal{A}}(W_{\mathcal{B}}^s)^{-1}$ and $W_{\mathcal{B}}^u$. The triangular region defined by S_1, S_2 and S_3 maps to the right hatched region. Thus the triangular region defined by $F_{\mathcal{B}3}$, S_1 and S_3 maps onto the union of the right and left hatched region, defined by $F_{\mathcal{B}3}$, $M_{\mathcal{A}}^r(S_3)$ and $M^r\mathcal{B}(S_2)$. Thus, the right and left hatched region is a trapping region of the 2D-map. Notice also that the 2D-map in the trapping region is invertible. This is a necessary consequence of the generation of the map from a differential equation and the projection procedure to two dimensions.

5.5. Transversal homoclinic points

A transverse homoclinic point is a point of a map where the stable and unstable manifolds of a fixed-point cross. The existence of transverse homoclinic points is often considered an important feature. This is because, if a map has a transverse homoclinic point and certain technical requirements are also met, the map has an invariant Cantor set on which it is topologically conjugate to a full shift map [35]. However, since the Cantor set is not necessarily attracting, the existence of a transverse homoclinic point may have limited relevance to the asymptotic dynamics.

Although, it is often a difficult matter to compute transverse homoclinic points, in the present case, the computation is straightforward. Since in the 2D-plane, lines map to lines, an analytical formula giving the coordinates of the PiP (primary intersection point of $W_{\mathcal{A}}^u$ and $W_{\mathcal{A}}^s$) and $PiP^{(-1)}$, is immediate (from the mapping of the vertical and horizontal axis, respectively)

$$
\text{PiP} = \begin{bmatrix} 0 \\ \dfrac{b_{11}b_{23} - b_{13}b_{21}}{b_{11}b_{33} - b_{31}b_{13}} \end{bmatrix} \approx \begin{bmatrix} 0 \\ -0.0008337 \end{bmatrix} \quad \text{and} \quad \text{PiP}^{(-1)} = \begin{bmatrix} -\dfrac{b_{13}}{b_{11}} \\ 0 \end{bmatrix} \approx \begin{bmatrix} -0.0025 \\ 0 \end{bmatrix}. \tag{5.2}
$$

The forward and backward iterations of the PiP give the whole set of homoclinic points

Fig. 5(a) indicates schematically the mapping of the unstable manifold $W_{\mathcal{A}}^u$ in the 2D-plane. To the left of the separating boundary b, map $M_{\mathcal{B}}^r(x)$ has to be applied wheras to the right of b, $M_{\mathcal{B}}^r(x)$ is applied. The region given to the right of the inverse of the boundary $M_{\mathcal{A}}^r(b)^{-1}$ determines the exit region of domain $\mathcal{A}$. The line piece L_1 on $W_{\mathcal{A}}^u$ is mapped onto itself and L_2. Line piece L_2 is mapped onto L_3 in $\mathcal{B}$-domain which is then mapped back to $\mathcal{A}$ onto L_4. Mapping L_4 gives L_5 which is contained in $\mathcal{A}$ as well as in $\mathcal{B}$-domain, hence a splitting occurs.

Since the ratio of contraction along $W_{\mathcal{A}}^s$ to the expansion in $W_{\mathcal{A}}^u$ is $\lambda_1/\lambda_2 \approx 300$, the iterated line segments like L_5 will lie very close to $W_{\mathcal{A}}^u$. This is shown in Fig. 5(b) which gives the numerically computed dynamics. Fig. 5(c) gives the retrun map obtained when plotting $y_1^{(k+1)}$ as a function of $y_1^{(k)}$. The attraction to the stable manifold $W_{\mathcal{A}}^s$ combined with the expansion and inversion of this manifold are the domainant features of the asymptotic dynamics.

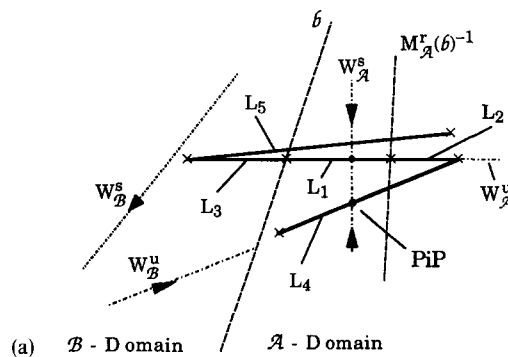(a) $\mathcal{B}$ - Domain $\mathcal{A}$ - Domain

Fig. 5. (a) A schematic drawing of four successive mappings of the line section L_1 on the unstable manifold $W_{\mathcal{A}}^u$ in the 2D-plane. L_1 is mapped onto itself and L_2, L_2 is mapped to L_3 in $\mathcal{B}$-domain. L_3 is mapped to L_4, which in turn is mapped to L_5. The end points of each line segment are indicated by the symbol $\times$. The maps in the $\mathcal{A}$-domain have inversions so that for example the left-most point on L_4 maps to the right-most point on L_5. (b) The appearance of the strange attractor on the 2D-plane when plotting 500 iterations. (c) The return map obtained when plotting $y_1^{(k+1)}$ as a function of $y_1^{(k)}$.
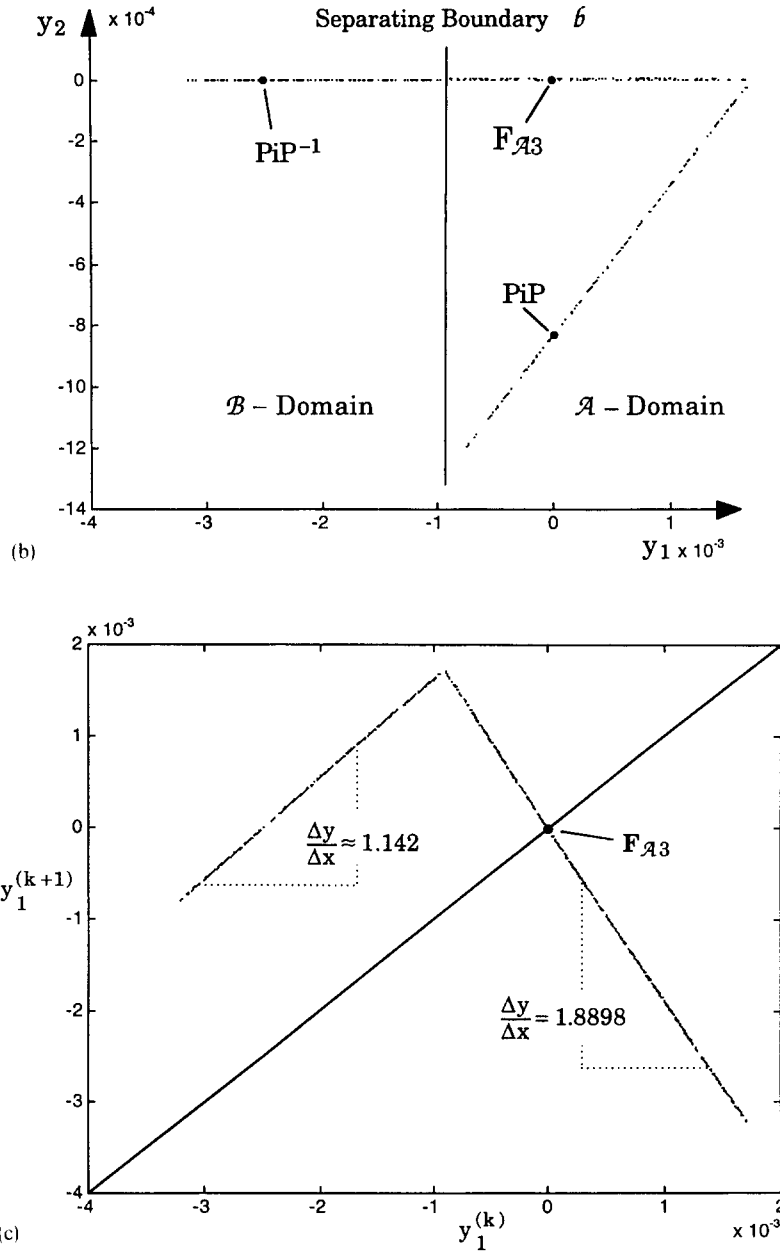
(b)

(c)

Fig. 5. Continued

6. A piecewise affine map

The two-dimensional map in Section 5 displays a transverse homoclinic intersection between the stable and unstable manifold of F_{A3}.

Although this guarantees an invariant chaotic set [35,36], it tells, in general, nothing about the attracting set. In our example the dynamics in the attracting set is dominated by the strong contraction to the unstable maniflod W^u_A

and the expansion along it. We may distill this situation into a piecewise affine map, given by

Region $\mathcal{A}$: $x^{(k)} \geq -1$ Region $\mathcal{B}$: $x^{(k)} < -1$

$$\begin{bmatrix} x \\ y \end{bmatrix}^{(k+1)} = \begin{bmatrix} -2 & 0 \\ 0 & -\varepsilon \end{bmatrix} \begin{bmatrix} x \\ y \end{bmatrix}^{(k)} \qquad \begin{bmatrix} x \\ y \end{bmatrix}^{(k+1)} = \begin{bmatrix} m & 0 \\ 1 & -\varepsilon \end{bmatrix} \begin{bmatrix} x \\ y \end{bmatrix}^{(k)} + \begin{bmatrix} m \cdot a \\ 1 \end{bmatrix} \qquad (6.1)$$

where $|\varepsilon| \ll 1$ gives the coupling between variables x and y.

As before the x-axis is the unstable manifold of the fixed point at $(0, 0)$, and the y-axis is the stable manifold. Notice that all points for which $x^{(k)} < -1$, map in one iteration to region $\mathcal{A}$, and all points in $\mathcal{A}$, except those on $W^s_{\mathcal{A}}$, will eventually map to region $\mathcal{B}$. Therefore, any periodic orbit must have at least one iterate in $\mathcal{B}$. If the relationship $m = 2/(a - 1)$ is satisfied then the mapping is continuous at the boundary. Assume the system starts close to the fixed point at $(0, 0)$. The largest x-coordinate in $\mathcal{A}$ is $x = 2$, so that $x = -4$ is the most negative x-coordinate in $\mathcal{B}$. Let c be the x-coordinate of the iterate of this point. Once c is chosen, the parameter $a = (8 - c)/(2 - c)$ and $m = \frac{1}{3}(2 - c)$ are determined. If $-1 \leq c < 0$ the situation is qualitatively similar to the 2D-map in Section 5.3. There is again a transverse homolinic point. However, the map in Eq. (6.1) is not 1:1, so that there is not a unique inverse. Fig. 6(a) shows the numerically computed attractor for a chosen parameter set.

If $\varepsilon = 0$, we can consider the x-coordinate of successive iterates independent of the y-coordinate. The map of $x^{(k+1)}$ vs. $x^{(k)}$ is a tent map, Fig. 6(b), see also [34]. The map is bounded in the interval $-4 \leq x^{(k)} \leq 2$, and under iteration the map is expanding in $\mathcal{A}$ since the slope $= -2$. In $\mathcal{B}$, the x-coordinate is multiplied by m. Since the system stays in $\mathcal{B}$ for at the most one iteration, a lower bound for the average Lyapunov exponent h is:

$h > \frac{1}{2}(\log| - 2| + \log|m|)$ with $m = 0.9333 \implies h = 0.3121$. Therefore, there is sensitive dependence to initial conditions and chaotic dynamics.

For $\varepsilon \neq 0$, the dynamics is more delicate. Chaotic dynamics must persist but the attractor displays subtle geometric features that are not fully understood.
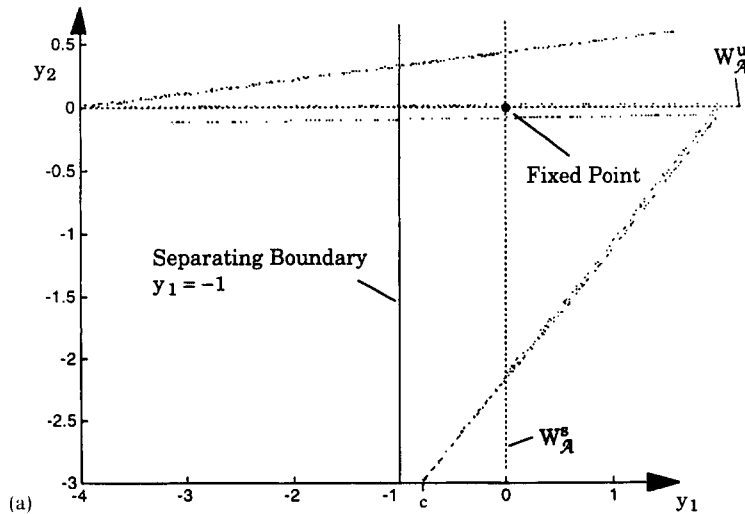

Fig. 6. (a) The iterations of Eq. (6.1) with $c = -0.8$, $\varepsilon = 0.2$, $a = 3.1429$ and $m = 0.9333$. 700 iterates are plotted after a transient period. (b) The corresponding return map of Eq. (6.1) obtained when plotting $x^{(k+1)}$ as a function of $x^{(k)}$.
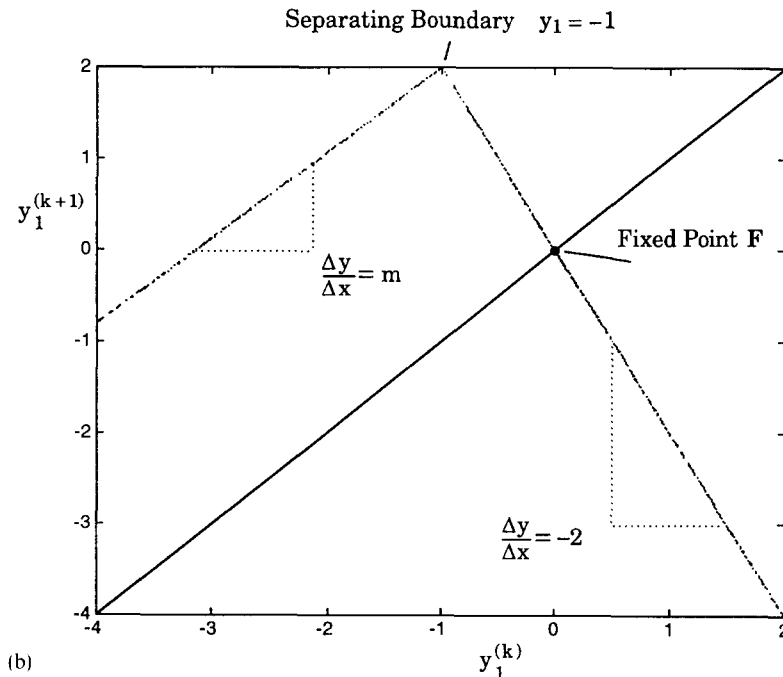
Fig. 6. Continued

7. Discussion

Although we have focused on a single example, the class of equations represented by Eq. (2.1), from which this example is taken, have been proposed as theoretical models of gene regulatory systems and neural networks. There is an embarrassingly sparse set of examples illustrating direct applications of a mathematical approach in concrete biological situations (see [1,37]). We do not know if this reflects limitations of the equations imposed by their simple structure, or whether it is due to unfamiliarity of the mathematics to biologists. However, the fact that many proteins show a switch-like change in their chemical properties, and that often their primary function appears to be the transfer and processing of information, suggests a mathematical description in form of Eq. (2.1). Protein molecules and genes are, in principle, able to perform a great variety of computational operations, e.g. OR, AND, NOT [3]. Independent of biology, the equations reflect the dynamics of asynchronous switching networks, and the methods presented here might have practical implications for engineering applications [19,38,39].

Although there has been considerable analysis of such systems, much of this work has been focused on conditions for stability of steady states [1,5,16,40–42]. In contrast, the current paper focuses on dynamical properties. A number of open questions remain. For instance, is it possible to predict the range of possible behavior of a system (including chaos) based on the hypercube representation? What bifurcations are observed as the focal points are shifted? Are there any practical or mathematical implications of the observation that we are able to classify high-dimensional systems that generate chaos?

Although we are still far away from a complete understanding of this kind of system, the geometric structure invites a variety of mathematical results. see [11,12,20,22]. Some important features of these flows are:

(1) The flows can be classified by directed graphs on an n-dimensional hypercube. In the case in which the sign of $\alpha_i(X)$ is not a function of i, each edge on the hypercube is directed in a unique orientation. Thus, if there are n variables there is a maximum of $2^{n \times 2^{n-1}}$ different labelings of the cube (neglecting possible symmetries).

(2) Flows in the phase space are piecewise linear and piecewise focused. This structure enables exact integration of the equations by composition of fractional linear maps.

(3) A stable vertex (all arrows are directed towards it) in the hypercube is associated with a stable steady state in the differential equations.

(4) A cycle on the hypercube is associated with a Poincaré map that is a fractional linear map on an appropriate subspace (= wall $\mathcal{W}$). A necessary requirement for a periodic orbit or an attracting focus along the state space specified by a cycle, is the existence of an eigenvector of the Poincaré map in its domain of definition. An additional requirement, though not sufficient, for the existence of closed trajectories is that the associated eigenvalue is greater than one. An analytical expression for the stable and unstable manifolds of a fixed point can be derived giving information about stability of the orbit. This is useful for analyzing complex dynamics.

(5) Multiple cycles through a vertex in the hypercube may be associated with chaos, but the necessary conditions for chaos are not known. However, the hypercube representation gives a natural way to classify chaos in this class of equations.

These transparent geometric properties of PL equations should encourage further development of this analysis.

Acknowledgements

Appendix A. Probabilistic approach

We now consider a Markovian model in which each edge in the state transition diagram is associated with a transition probability. Consider box (0000) having three exit walls to (0001), (0010) and (0100). Hence, there exists a certain volume in box (0000) inside which a trajectory will go to (0001). A measure of the transition probability from (0000) to (0001) is given by the appropriate relative volume fraction of the box. The volume V_i in a box that exits through wall $\mathcal{W}_i = \{x_i = 0\}$ is derived from the focal point coordinate f(box). The transition probability of crossing wall $\mathcal{W}_i$ is then

$$P(\mathcal{W}_i) = \frac{|f_i|}{\sum_{j=1}^{k} |f_j|} \tag{A.1}$$

where f_i is the ith coordinate of f, and the sum $j = \{1, \ldots, k\}$ runs over the k exit walls of the box.

To demonstrate (A.1) assume the system is n-dimensional with equal relative decay rate. Without loss of generality, let $1 \ldots 1$ be the branching box. Let the system be in the 'entrance' wall, $\mathcal{W}_{\text{ent}} = \{x_1 > 0, \ldots, x_{n-1} > 0, \ x_n = 0\}$. Suppose there are $k < n$ exits to adjacent boxes denoted by $01 \ldots 1$, and $101 \ldots 1$, etc. Consequently, the branching box is divided into k volumes V_i such that initial values in volume V_i produce trajectories entering the exit wall $\mathcal{W}_i$. Assume the system leaves the branching box in direction of box $101 \ldots 1$, i.e. $\mathcal{W}_2 = \{x_1 > 0, x_2 = 0, \ldots, x_n > 0\}$. Let $\mathcal{W}_2^{-1}$ be that part of $\mathcal{W}_{\text{ent}}$ which mapped forward gives $\mathcal{W}_2$. Volume V_2 is given by the vectors spanning $\mathcal{W}_2$ and $\mathcal{W}_2^{-1}$.

$\mathcal{W}_2$ is spanned by the unit vectors $e_i = \{x_i = 1, \ x_j = 0, \ i \neq j\}$ with $i \in \{1, 3, \ldots, n\}$ whereas $\mathcal{W}_2^{-1}$ is spanned by e_i, $i \in \{1, 3, \ldots, n-1\}$ *and* vector s. Vector s is the backwards mapping of e_n from $\mathcal{W}_2$, or the other way round,

when s mapped forward must give e_n. Applying Eq. (2.4) it is easy to check that $s = -[f_1, f_2, f_3, \ldots, f_{n-1}, 0]^t$ gives ce_n, where $c > 0$:

$$M(s) \cong \frac{Cs}{1 + c^t s}$$

$$= \frac{1}{1 + c^t s} \begin{bmatrix} 1 & -f_1/f_2 & & \\ & -f_3/f_2 & 1 & \\ & \vdots & & \ddots \\ & -f_n/f_2 & & 1 \end{bmatrix} \begin{bmatrix} -f_1 \\ -f_2 \\ \vdots \\ -f_{n-1} \\ 0 \end{bmatrix}$$

$$= c \begin{bmatrix} 0 \\ 0 \\ \vdots \\ 0 \\ 1 \end{bmatrix}. \tag{A.2}$$

Realize that s is independent of which exit wall is chosen. The volumes V_i are then easily computed by taking the determinant of the spanning vectors, i.e. $\mathrm{vol}(V_i) = |\det(e_i, s)| = |f_i|$, where e_i span $\mathcal{W}_i$. To obtain the transition probability $P(\mathcal{W}_i)$ the volume elements have to be normalized, i.e. $\sum_{j=1}^k |f_j| = 1$, hence the division in (A.1).

References

[1] R. Thomas and R.D. Ari, Biological Feedback (CRC Press, Boca Raton, 1990).
[2] S.A. Kauffman, The Origin of Order (Oxford University Press, Oxford, 1993).
[3] D. Bray, Nature 376 (1995) 307.
[4] S.A. Kauffman, J. Theor. Biol. 22 (1969) 437.
[5] J.J. Hopfield, Proc. Natl. Acad. Sci. (USA) 79 (1982) 2554.
[6] J.J. Hopfield, Proc. Natl. Acad. Sci. (USA) 81 (1984) 3088.
[7] D.R. Rigney, Bull. Classe Sci. Acad. Roy. Belge. 6 (1977) 516.
[8] R. Thomas, J. Theor. Biol. 153 (1991) 1.
[9] L. Glass and S.A. Kauffman, J. Theor. Biol. 34 (1972) 219.
[10] L. Glass and S.A. Kauffman, J. Theor. Biol. 39 (1973) 103.
[11] L. Glass and J.S. Pasternack, J. Math. Biol. 6 (1978) 207.
[12] T. Mestl, E. Plahte and S.W. Omholt, Dyn. Stab. Systems 2 (1995) 179.
[13] E. Plahte, T. Mestl and S.W. Omholt, Dyn. Stab. Systems 9 (1994) 275.
[14] S.I. Amari, Biol. Cybernetics 26 (1977) 175.
[15] B.C. Goodwin, in: Advances in Enzyme Regulation, ed. G. Weber, Vol. 3 (Pergamon, Oxford, 1965).
[16] J.J. Hopfield and D.W. Tank, Science 233 (1986) 625.
[17] J.M. Mahaffy, J. Math. Anal. Appl. 74 (1980) 72.
[18] I. Morishita and A. Yajima, Kybernetic 11 (1972) 156.
[19] J.M. Zurada, Introduction to Artificial Neural Systems (West, New York, 1992).
[20] L. Glass, J. Theor. Biol. 54 (1975) 85.
[21] T. Mestl, E. Plahte and S.W. Omholt, J. Theor. Biol. 176 (1995) 291.
[22] L. Glass in: Statistical Mechanics and Statistical Methods in Theory and Application, ed. U. Landman (Plenum, New York, 1977) p. 585.
[23] L. Glass, in: Dynamical Systems and Cellular Automata, ed. J. Demongeot, E. Goles and M. Tchuente (Academic Press, London, 1985) p.197.
[24] E.H. Snoussi, Dyn. Stab. Systems 4 (1989) 189.
[25] E.H. Snoussi and R. Thomas, Bull. Math. Biol. 55 (1992) 973.
[26] P.K. Das II, W.C. Schieve and Z. Zeng, Phys. Lett. A 161 (1991) 60.
[27] P.K. Das II and W.C. Schieve, Physica D 1 (1995) 14.

[28] T.B. Kepler, S. Datt, R.B. Meyer and L.F. Abbott, Physica D 46 (1990) 449.

[29] K.E. Kürten and J.W. Clark, Phys. Lett. A 7 (1986) 413.

[30] J.E. Lewis and L. Glass, Internat. J. Bifurc. Chaos 2 (1991) 477.

[31] J.E. Lewis and L. Glass, Neural Comput. 4 (1992) 621.

[32] H. Sompolinsky and A. Crisanti, Phys. Rev. Lett. 3 (1988) 259.

[33] E. Ott, Chaos in Dynamical Systems (Cambridge Uni- versity Press, Cambridge, 1993).

[34] R. Devaney, An Introduction to Chaotic Dynamical Systems (Benjamin/Cummings, Amsterdam, 1986).

[35] S. Wiggins, Introduction to Applied Nonlinear Dynamical Systems and Chaos (Springer, Berlin, 1990).

[36] J. Hale and H. Koçak, Dynamics and Bifurcation (Springer, Berlin, 1991).

[37] F.A. Bignone, Fed. Am. Soc. Exp. Biol. 2 (1988) 5.

[38] H.P. Graf, L.D. Jackel, R.E. Howard, B. Straughn, J.S. Denker, D.M. Hubbard, D.M. Tennant and D. Scharz, in: Neural Networks for Computing (Snowbird, 1986), ed. J.S. Denker (American Institute of Physics, New York, 1986) p.182.

[39] J. Herz, A. Krogh and R.G. Palmer, Introduction to the Theory of Neural Computation (Addison-Wesely, New York, 1991).

[40] D.J. Amit, Modelling Brain Function: The World of Attractor Neural Networks (Cambridge University Press, Cambridge, 1989).

[41] J.J. Hopfield, D.I. Feinstein and R.G. Palmer, Nature 304 (1983) 158.

[42] I. Kanter and H. Sompolinsky, Phys. Rev. A 35 (1987) 380.